

From vortex molecules to the Abrikosov lattice in thin mesoscopic superconducting disks

L. R. E. Cabral,* B. J. Baelus,[†] and F. M. Peeters[‡]

*Departement Natuurkunde, Universiteit Antwerpen (Campus Drie Eiken),
Universiteitsplein 1, B-2610 Antwerpen, Belgium*

(Dated: July 2, 2018)

Stable vortex states are studied in large superconducting thin disks (for numerical purposes we considered with radius $R = 50\xi$). Configurations containing more than 700 vortices were obtained using two different approaches: the nonlinear Ginzburg-Landau (GL) theory and the London approximation. To obtain better agreement with results from the GL theory we generalized the London theory by including the spatial variation of the order parameter following Clem's ansatz. We find that configurations calculated in the London limit are also stable within the Ginzburg-Landau theory for up to ~ 230 vortices. For large values of the vorticity (typically, $L \gtrsim 100$), the vortices are arranged in an Abrikosov lattice in the center of the disk, which is surrounded by at least two circular shells of vortices. A Voronoi construction is used to identify the defects present in the ground state vortex configurations. Such defects cluster near the edge of the disk, but for large L also grain boundaries are found which extend up to the center of the disk.

PACS numbers: 74.20.De, 74.25.Dw, 74.25.Ha

I. INTRODUCTION

Vortices appear in several branches of physics, such as fluid dynamics,¹ superfluidity,² Bose-Einstein (B-E) condensates,^{3,4,5} and superconductivity.^{6,7} The vortex is usually described by a field (for instance, the velocity field) which diverges as r^{-1} as one approaches its core.⁸ They can be treated as quasiparticles, since they can be created or destroyed, they interact with each other and with the interfaces. Unlike in fluid dynamics, in superfluids (including here superconductors and B-E condensates) vortices are quantized objects. In superconductors, for example, they carry a magnetic flux which is a multiple of the flux quantum, $\Phi_0 = hc/2e$, and are characterized by a core of area ξ^2 – where the superconductivity is highly depreciated – surrounded by superconducting currents (screened at distances of order λ). Here, ξ is the coherence length. They have been intensively studied, since Abrikosov⁶ predicted their existence from the solution of the Ginzburg-Landau (GL) equations in a type-II superconductor for $H_{c1} < H < H_{c2}$ (see also Refs. 9 and 10). In an infinite, and defect free superconductor, vortices arrange themselves in an hexagonal (Abrikosov) lattice.

A detailed phenomenological description of the superconducting state can be derived from the GL theory,¹¹ by means of two parameters: the complex order parameter, Ψ , which is related to the superconducting electron density, and the vector potential, \mathbf{A} . For $H_{c1} \leq H \ll H_{c2}$, each vortex can be viewed as a particle, since inter-vortex separations, a , are such that $\xi \ll a \sim \lambda$ – assuring that vortex cores do not overlap – and the major role between vortex-vortex interactions is played by the superconducting shielding currents. In such cases the London limit turns out to be a good approximation of the GL theory, becoming better for higher values of κ (see for example Refs. 7,12,13,14). In this approximation, the supercon-

ducting electron density is considered constant throughout the entire superconductor and the vortex cores are represented by singularities in the phase of the order parameter. This allows to treat vortices as particles.

In a thin film of thickness d , the effective magnetic field shielding length turns out to be the effective penetration depth, $\Lambda = \lambda^2/d$, instead of λ .¹⁵ At distances $r \ll \Lambda$ the electromagnetic interaction is still logarithmic, as in the three dimensional case, but with screening length Λ [However the perpendicular magnetic field and the shielding currents decay as r^{-3} and r^{-2} far away from the vortex core for $r \ll \Lambda$, instead as $\exp(-r/\lambda)$ in the bulk case.] Similarly as in the bulk case, in a thin film vortices also form an hexagonal Abrikosov lattice.¹³

In mesoscopic superconductors both the geometry and size of the specimen influence the vortex configurations, due to the interaction between vortices and the surface. Therefore, for small enough samples (with sizes comparable to ξ), the conventional hexagonal lattice predicted by Abrikosov no longer exists, and vortex configurations adjust to the sample geometry, yielding some kind of vortex molecule states.^{16,17,18,19,20} For example, vortices arrange themselves in ringlike structures in disks with radii (R) a few times ξ .^{18,19,20,21,22,23,24,25,26,27,28,29,30} Such patterns show similarities to what is observed in electrons in artificial atoms, where particles obey specific rules for shell filling and exhibit magic numbers. Nevertheless when overlapping of vortices starts to take place, discrepancies between vortices and a picture based on particles arise, such as the formation of giant vortex states. Also, vortex-antivortex configurations may become possible for non circular geometries.^{31,32,33}

Within the London limit the vortex interaction potential in a thin disk of arbitrary radius was first calculated by Fetter³⁴. Also in the London limit, vortex configurations up to $L = 8$ were studied by Buzdin and Brison³⁵ for $\Lambda \gg R$ (where demagnetization effects can be ne-

glected). In the latter limit it is possible to substitute the interaction between the vortices and the disk border by the interaction between vortices and their images (see also Ref. 36). Within the London limit one is able to find analytical expressions for the energy and forces of an arbitrary arrangement of vortices inside the disk, since vortices can be treated as particles. Vortices considered as particles were also studied by Monte Carlo and Molecular Dynamics simulations. In Ref. 37 vortex configurations with up to 2000 vortices were studied and an hexagonal lattice was found for thin disks, although they did not consider the vortex interaction with the disk edge. Vortex molecules in long cylinders with radius much larger than λ were studied by Venegas and Sardella.³⁸ Other geometries were investigated in Refs.^{39,40}, for example.

In this paper we will study multivortex states where many vortices nucleate, yielding a triangular lattice in the center of the disk and a ringlike structure close to the edges. Within the GL framework several other works have been reported regarding vortex states in thin disks,^{18,19,21,22,23,24,25,26,27,28,29,30} but they were limited to much smaller disk radius. In such small systems the formation of multivortex states with high vorticity is not allowed and, consequently, it was not possible to study the transition from a ringlike structure to an Abrikosov lattice, which is the subject of the present paper.

This paper is organized as follows. The theoretical approach is described in Section II. In Section III low vorticity states obtained within the GL and the London frameworks are compared. In Sections IV and V configurations with up to 700 vortices are investigated, respectively, by showing the existence of an Abrikosov lattice in the center of the disk and by examining the role of topological defects in the lattice in order to adjust the hexagonal lattice to the radial symmetry close to the disk edge. Surface superconductivity in the $R = 50\xi$ disk is briefly analyzed in Section VI. Our conclusions are given in Section VII.

II. THEORETICAL APPROACH

For our numerical calculation we used a thin disk of radius $R = 50\xi$ and thickness d , in which $\Lambda = \lambda^2/d \gg \xi \gg d$, surrounded by vacuum and in the presence of a uniform perpendicular magnetic field \mathbf{H}_0 . In this regime, the demagnetization effects can be neglected, allowing one to assume $\mathbf{H} \approx \mathbf{H}_0$. Vortex states in mesoscopic thin disks were investigated by us using both the Ginzburg-Landau (GL) theory and the London approximation with the London gauge $\nabla \cdot \mathbf{A} = 0$. Dimensionless variables are used, i.e., the distance is measured in units of the coherence length ξ , the vector potential in $c\hbar/2e\xi$ and the magnetic field in $H_{c2} = c\hbar/2e\xi^2 = \kappa\sqrt{2}H_c$. The average energy density is written in units of $H_c^2/8\pi$ (we shall refer to it as simply the energy of the system). Also, the vorticity or the number of vortices in the system will be denoted by L (an analogue to the total angular momentum).^{20,24}

Moreover, whenever the distinction among different configurations with the same L would be necessary, we use the notation presented in Ref. 20 to denote the vortex configurations, e.g., for $L = 6$, (1, 5) means 1 vortex in the center with 5 around it, and (6) represents 6 vortices with none of them in the center of the disk.

In the framework of the GL theory, the GL equations are solved numerically according to the approach of Schweigert and Peeters.^{23,24} As we are in the limit ($d \ll \xi, \lambda$), the Ginzburg-Landau equations can be averaged over the disk thickness, leading to the following system of equations,

$$(-i\nabla_{2D} - \mathbf{A})^2 \Psi = \Psi (1 - |\Psi|^2) \quad (1)$$

and

$$-\Delta_{3D} \mathbf{A} = \mathbf{j}, \quad (2)$$

where the supercurrent density is defined by the following,

$$\begin{aligned} \frac{\kappa^2}{d} \mathbf{j} &= \delta(z) \left[\frac{1}{2i} (\Psi^* \nabla_{2D} \Psi - \Psi \nabla_{2D} \Psi^*) - |\Psi|^2 \mathbf{A} \right] \\ &= \delta(z) |\Psi|^2 (\nabla_{2D} \theta - \mathbf{A}) = \delta(z) |\Psi|^2 \mathbf{\Pi}. \end{aligned} \quad (3)$$

Above, the superconducting wavefunction, $\Psi = |\Psi|e^{i\theta}$, satisfies the boundary conditions $(-i\nabla_{2D} - \mathbf{A})\Psi|_n = 0$ normal to the sample surface and $\mathbf{A} = \mathbf{A}_0 = \frac{1}{2}H_0\rho\hat{\phi}$ (since demagnetization effects can be neglected). Here $\hat{\phi}$ is the unit vector in the azimuthal direction. The indices 2D, 3D refer to two- and three-dimensional operators, respectively. The dimensionless GL energy density is given by

$$\mathcal{G} = \mathcal{G}_{\text{core}} + \mathcal{G}_{\text{em}}, \quad (4a)$$

where

$$\mathcal{G}_{\text{core}} = \frac{1}{V} \int_V \left[-2|\Psi|^2 + |\Psi|^4 + 2(\nabla_{2D} |\Psi|)^2 \right] dV, \quad (4b)$$

$$\mathcal{G}_{\text{em}} = \frac{1}{V} \int_V \left[2|\Psi|^2 \Pi^2 + 2\kappa^2 (\mathbf{H} - \mathbf{H}_0)^2 \right] dV, \quad (4c)$$

are the core and the electromagnetic energies, respectively, and the integrations are to be performed over the sample volume V . As demagnetization effects can be disregarded, the above equation reduces to

$$\mathcal{G} = -\frac{1}{V} \int_V |\Psi|^4 dV, \quad (5)$$

which was actually the expression used to compute the energy of the vortex configurations within the GL theory. For now on the symbol ∇ will be used for the two-dimensional gradient operator.

The system of Eqs. (1,2) were solved by using the approach of Ref.²⁴ for circular disks. A finite-difference representation for the order parameter is used on an uniform 2D square grid (x,y), with typically 512×512 grid

points for the area of the superconductor, which allows to have at least 5 grid points inside a length of the order of ξ . We also use the link variable approach,⁴¹ and an iteration procedure based on the Gauss-Seidel technique to find Ψ . Starting from different randomly generated initial conditions and at some specified magnetic field, the steady-state solutions of Eqs. (1,2) yield different vortex configurations, either stable or meta-stable states.

In the London approximation, the order parameter is considered uniform throughout the disk, except for small regions with areas of the order of ξ^2 , where it drops to zero. This can only be accomplished when $\kappa \gg 1$. Then the energy of the system is purely electromagnetic and it is given by the sum of the supercurrent and the magnetic field energies

$$\mathcal{G}_L = \frac{2\kappa^2}{V} \int dV \left[(\mathbf{H} - \mathbf{H}_0)^2 + \kappa^2 |\mathbf{j}|^2 \right]. \quad (6)$$

Notice that this expression is a particular case of Eq. (4c) which is obtained by putting $|\Psi|^2 = 1$ everywhere inside the disk. In the presence of L vortices, situated at $\boldsymbol{\rho}_i$ $\{i = 1, 2, \dots, L\}$, the London equation can be written as

$$\mathbf{J} = \frac{d}{\kappa^2} (\boldsymbol{\nu} - \mathbf{A}), \quad (7)$$

where

$$\boldsymbol{\nu} = \sum_{i=1}^L \left[\Phi(|\boldsymbol{\rho} - \boldsymbol{\rho}_i|) - \Phi(|\boldsymbol{\rho} - (R/\rho_i)^2 \boldsymbol{\rho}_i|) \right], \quad (8)$$

with $\boldsymbol{\rho}_i = (x_i, y_i)$ the position of the vortices, $\mathbf{J} = \int_0^d dz \mathbf{j} \approx \mathbf{j} d$, and $\Phi(\rho) = \hat{\phi}/\rho$. The vortex images at $(R/\rho_i)^2 \boldsymbol{\rho}_i$ appear in Eq. (8) in order to fulfill the boundary condition³⁵ $\mathbf{J}(R) \cdot \hat{\rho} = 0$. Instead of writing Eq. (7) for the vector \mathbf{J} , one may use the streamline function, $g(\boldsymbol{\rho})$, related to the supercurrent by $\mathbf{J} = \nabla \times (\hat{z}g)$ ($g(\boldsymbol{\rho})$ can be regarded as a local magnetization in the thin film.⁴²) At the boundary $g(R, \phi) = \text{const}$, but, as the value of this constant is arbitrary, one can impose $g(R, \phi) = 0$. Therefore, Eqs. (7) and (8) can be expressed as,

$$g(\boldsymbol{\rho}) = \frac{d}{\kappa^2} \left[\sum_{j=1}^L \ln \left(\frac{|\boldsymbol{\rho} - (R/\rho_j)^2 \boldsymbol{\rho}_j| \rho_j}{|\boldsymbol{\rho} - \boldsymbol{\rho}_j| R} \right) - \frac{H_0}{4} (R^2 - \rho^2) \right]. \quad (9)$$

Notice that Eq. (7) can also be understood as the limiting case of the GL equations if one considers $|\Psi| = 1$ and $\nabla\theta = \boldsymbol{\nu}$. Therefore, while vortices are well apart from each other (and also the boundary), there exists a relation between the streamline function defined above and the phase of the order parameter in the GL theory, i.e., one can define a complex function of which the real and imaginary parts are proportional to $g(\boldsymbol{\rho})$ and θ .³⁴

Since in our case ($\Lambda = \lambda^2/d \gg \xi \gg d$), demagnetization effects can be neglected²⁰ and one may write Eq. (6)

as

$$\begin{aligned} \mathcal{G}_L &= \frac{2\kappa^4}{Vd} \int d^2\rho |\mathbf{J}|^2 = \frac{2\kappa^4}{Vd} \int d^2\rho g(\boldsymbol{\rho}) \hat{z} \cdot \nabla \times \mathbf{J} \\ &= \frac{2\kappa^2}{V} \left[2\pi \sum_{i=1}^L g(\boldsymbol{\rho}_i) - H_0 \int d^2\rho g(\boldsymbol{\rho}) \right], \end{aligned} \quad (10)$$

where the integration is performed along the thin film plane, $z = 0$. Substituting Eq. (9) in this formula, and after some algebraic manipulation, the London energy is expressed by

$$\begin{aligned} \mathcal{G}_L &= \left(\frac{2}{R} \right)^2 \sum_{i=1}^L \sum_{j=1}^L \ln \left(\frac{r_j |\mathbf{r}_i - \mathbf{r}_j / r_j^2|}{|\mathbf{r}_i - \mathbf{r}_j|} \right) \\ &\quad - 2H_0 \sum_{i=1}^L (1 - r_i^2) + R^2 H_0^2, \end{aligned} \quad (11)$$

where we used $\mathbf{r}_i = \boldsymbol{\rho}_i/R$ to simplify the notation.

The divergence in Eq. (11) can be removed by considering a cut-off, in which for $i = j \rightarrow |\boldsymbol{\rho}_i - \boldsymbol{\rho}_j| = a\xi$ (in not normalized units) and a is a constant. The final expression for the London energy can be written as

$$\mathcal{G}_L = \sum_{i=1}^L \left(\epsilon_i^{\text{self}} + \epsilon_i^{\text{shield}} + \sum_{j=1}^{i-1} \epsilon_{ij} \right) + \epsilon^{\text{core}} + \epsilon^{\text{field}}, \quad (12a)$$

where

$$\epsilon_i^{\text{self}} = \left(\frac{2}{R} \right)^2 \ln(1 - r_i^2) \quad (12b)$$

is the interaction energy between the i^{th} vortex and the radial boundary of the superconductor,

$$\epsilon_i^{\text{shield}} = -2H_0 (1 - r_i^2) \quad (12c)$$

represents the interaction between the i^{th} vortex and the shielding currents, and

$$\epsilon_{ij} = \left(\frac{2}{R} \right)^2 \ln \left[\frac{(r_i r_j)^2 - 2\mathbf{r}_i \cdot \mathbf{r}_j + 1}{r_i^2 - 2\mathbf{r}_i \cdot \mathbf{r}_j + r_j^2} \right] \quad (12d)$$

is the repulsive energy between vortices i and j . Finally, $\epsilon^{\text{core}} = (2/R)^2 N \ln(R/a)$ and $\epsilon^{\text{field}} = R^2 H_0^2$ are the energies associated with the vortex cores and the external magnetic field, respectively.

Notice that \mathcal{G}_L allows one to treat the vortices as particles. Therefore, simulation techniques appropriate for systems of particles may be performed in order to find, for example, the ground state of the system.^{43,44,45} In this sense, the vortex system behaves (in the London approximation) similar to a two dimensional system composed of equally charged particles interacting through a repulsive logarithmic potential placed in parabolic potential well.^{46,47} Nevertheless, there is a fundamental difference between these two systems: the vortex system is confined

to the disk of radius R and the influence of the surface on the energy is clear from the terms containing vortex images, i.e., ϵ_i^{self} and ϵ_{ij} . Notice also that ϵ^{core} arises from the cut-off procedure and is therefore strongly dependent on the cut-off value $a\xi$ (we adopted $a = 1$ in the results shown below). The actual energy associated with vortex cores and with the spatial variation of the superconducting electron density ($|\psi(\boldsymbol{\rho})|^2$) should be evaluated by using the GL theory.

A thin disk with L vortices was simulated by using Eq. (12a). To investigate (meta-)stable states close to the equilibrium, we employed a procedure similar to the one described in Ref. 44. First L' vortices were distributed randomly inside the disk. Then, a Monte Carlo (MC) technique was used to make the system wander in the configurational space and arrive at a neighborhood of some minimum of \mathcal{G}_L . After typically 10^4 MC steps, we perform a molecular dynamics (MD) simulation starting from the final MC configuration. The final (meta-)stable state is achieved after about 10^6 MD steps. In order to find the ground state (or states with energies very close to it) this trial procedure was repeated more than 1000 times, each time starting with a different random distribution of L' vortices at a given magnetic field H_0 .

To implement the MD we time integrated the Bardeen-Stephen equation of motion⁴⁸

$$\eta \frac{d\boldsymbol{\rho}_i}{dt} = \mathbf{F}_i, \quad (13)$$

where i is the label of the i^{th} vortex, η is the viscous drag coefficient $\eta \sim \Phi_0 H_{c2} / \rho_n c^2$ (where ρ_n is the normal state resistivity). The forces acting on each vortex were obtained from $-\nabla_k \mathcal{G}_L(\boldsymbol{\rho}_i, \boldsymbol{\rho}_j)$, where \mathcal{G}_L is given by Eq. (12a) and $-\nabla_k$ is the gradient with respect to the coordinate $\boldsymbol{\rho}_k$. This yields a force per unit of volume,

$$\mathbf{F}_i = \mathbf{F}_i^s + \sum_{\substack{k=1 \\ k \neq i}}^L \mathbf{F}_{i,k}^{\text{int}}, \quad (14a)$$

which we express in units of $H_c^2 / 8\pi\xi$. Above, the first term describes the vortex interaction with the current induced by the external field and with the interface,

$$\mathbf{F}_i^s = \left(\frac{2}{R}\right)^3 \left(\frac{1}{1-r_i^2} - \frac{H_0 R^2}{2}\right) \mathbf{r}_i, \quad (14b)$$

and the second, the vortex-vortex interaction,

$$\mathbf{F}_{i,k}^{\text{int}} = \left(\frac{2}{R}\right)^3 \left(\frac{\mathbf{r}_i - \mathbf{r}_k}{|\mathbf{r}_i - \mathbf{r}_k|^2} - r_k^2 \frac{r_k^2 \mathbf{r}_i - \mathbf{r}_k}{|r_k^2 \mathbf{r}_i - \mathbf{r}_k|^2}\right). \quad (14c)$$

The simple Euler method was used to accomplish the time integration, but adopting a δt value small enough to avoid large variations of the vortex positions between two consecutive steps. Moreover, the dynamical matrix (the Hessian matrix of \mathcal{G}_L), whose elements are given by

$$\frac{\partial^2 \mathcal{G}_L}{\partial \rho_{\alpha,i} \partial \rho_{\beta,j}}, \quad (15)$$

was calculated for the final vortex configuration. In this equation, the Greek indexes stand for the components of the vector $\boldsymbol{\rho}_i$, while the Italic indexes are the labels for the vortices. The computation of the dynamical matrix eigenvalues allowed us to tell whether the given state was stable or unstable (for a stable state all the dynamical matrix eigenvalues must be non-negative). Unstable states were discarded.

One difficulty in simulating this system is the fact that both \mathcal{G}_L and the forces acting on the vortices diverge at the disk edge. To overcome this, during the MD simulation whenever a vortex was at a distance less than ξ from the disk edge, it is taken out from the system, i.e., this vortex disappears. Therefore, the final number of vortices may not be the same as in the beginning. This does not lead to any serious concern, since we collect all the final results from each trial and sort them in ascending order of energy. It also allows to compare energies of systems containing different number of vortices for the same external magnetic field and investigate which of them correspond to the lower energy, i.e., is the ground state.

III. LOW L -STATES: VORTEX MOLECULES

In this section we present the results calculated from the GL and London theories for low L -states for a thin disk of radius $R = 50\xi$. A comparison between ground states in the GL theory and the London approximation was done in Ref. 20, for the case of a small disk radius (i.e. $R = 6\xi$). In that case, it was not possible to study multivortex configurations for L -states above $L = 14$ since the calculated GL results showed only giant vortices. Moreover, above $L = 26$ the disk was driven to the *normal state*. In the present case, multivortex configurations are obtained for much higher L -states. This enabled us to compare large multivortex configurations calculated by both the GL theory and the London approximation, and investigate the transition to the Abrikosov lattice.

For $L = 1$ to $L = 9$, the lowest energy configurations consist of vortices distributed in regular polygons with 0 or 1 vortex in the center of the disk. This means that not many meta-stable states are close to the ground state, which makes the job of finding low energy configurations easier. In the London limit, this reduces Eqs. (12a)–(12d) to a simple form, which depends on only one free parameter,^{20,35} i.e., the radius of the ring which circumscribes the polygon, ρ_{ring} . The minimization problem is then straightforward. We also obtained the positions of the vortex ring by finding the roots of

$$\frac{1}{1-r^2} - h + \frac{N \pm 1}{2r^2} - \sum_{n=1}^{N-1} \frac{r^2 - \cos \phi_n}{1 + r^4 - 2r^2 \cos \phi_n} = 0, \quad (16)$$

which follows from the balance of forces acting on each vortex [cf. Eq (14)].³⁵ Here N is the number of vortices

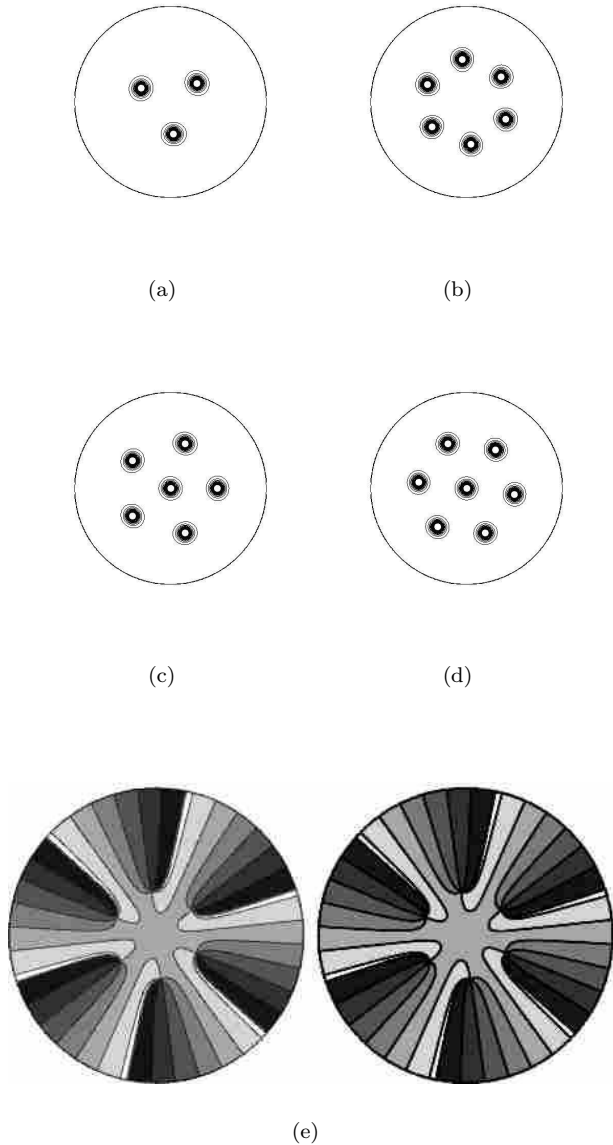


FIG. 1: Vortex configurations for $L = 3$ and $H_0 = 0.007$ (a), $L = 6$ and $H_0 = 0.01$ (b), $L = (1, 5)$ and $H_0 = 0.01$ (c), and $L = (1, 6)$ and $H_0 = 0.011$ (d). The black lines are the contour lines of $|\Psi(\mathbf{r})|^2$, whereas the white circles indicate the position of the vortices according to the London approximation. In (e) we show the phase of the order parameter for the $L = 6$ state at $H_0 = 0.022$ obtained from the GL equations (on the left) and from the London approximation (on the right).

on the ring (or the number of sides of the polygon), $r = \rho_{\text{ring}}/R$, $\phi_n = 2\pi n/N$, $h = H_0 R^2/2$ and the plus (minus) sign should be taken if there is one (zero) vortex in the center of the disk.

A comparison between the calculated GL and London vortex configurations is depicted in Fig. 1. The states $L = 3$ (Fig. 1(a)), $L = 6$ (Fig. 1(b)), $L = (1, 5)$ (Fig. 1(c)), and $L = 7$ (Fig. 1(d)) were obtained at

$H_0 = 0.007$, $H_0 = 0.01$, $H_0 = 0.01$, and $H_0 = 0.011$, respectively. The vortex positions practically coincide for the same configurations in both theories.

The agreement between the vortex positions yielded by both theories (at $H_0 \ll H_{c2}$) is related to the fact that the phase of the order parameter, θ , is well described as the imaginary part of the complex function

$$\Omega = \sum_{j=1}^L \ln \left[\left(\frac{\zeta - (R/\zeta_j)^2 \zeta_j}{\zeta - \zeta_j} \right) \frac{\rho_j}{R} \right] - \frac{H_0}{4} (R^2 - \rho^2), \quad (17)$$

for sufficiently small magnetic fields,³⁴ where $\zeta = \rho e^{i\phi} = x + iy$ is the representation of the vector $\boldsymbol{\rho}$ in the complex ζ -plane. But $(d/\kappa^2) \text{Re}\{\Omega\}$ is simply the streamline function [cf. Eq. (9)] calculated in the London limit. That is greatly responsible for the fact that ρ_{ring} is virtually the same in both theories for $H_0 \ll H_{c2}$. Fig. 1(e) presents the numerically calculate phase of the order parameter (left) and the theoretical one obtained from the imaginary part of Eq. (17) (right) for the state with $L = 6$ at $H_0 = 0.022$.

The dependence of ρ_{ring} upon H_0 is shown in Fig. 2(b) obtained within the GL (squares) and the London limit (solid line) for the $L = 1, (2), (3), (4), (5), (6), (1, 6), (1, 7)$ states. Both theories predict the same values of ρ_{ring} and, thus, the same stable configurations, as function of H_0 . Fig. 2(b) also shows the radial position over which a given regular polygon configuration is not stable (dashed lines) as function of H_0 (obtained in the London limit). The magnetic field in which the stable and unstable ρ_{ring} lines start to depart from each other (open circles) mark the onset of stability for each configuration. The unstable ρ_{ring} lines merge to

$$R \sqrt{1 - \frac{2}{H_0 R^2}}. \quad (18)$$

This is simply the position after which the attractive force acting on each vortex by its own image becomes larger than the force produced by the shielding currents (which pulls the vortices inside), as can be easily demonstrated from Eqs. (14a) and (14b) for one vortex. It is also important to take into account the vortex interaction with the disk edge for sufficiently low fields. This can be noticed from the difference between the stable ρ_{ring} and the dotted lines in Fig. 2(b), which depicts the position at which the respective regular polygon configuration would sit if there were no vortex images [from Eq. (16) in the absence of vortex images, ρ_{ring} would be given by $\sqrt{(N \pm 1)/H_0}$, where the $+$ ($-$) sign should be considered for one (zero) vortex in the center].

The free energies within the GL (thick lines) theory and the usual London limit (dashed line) are depicted in Fig. 2(a) for $L = 0 \rightarrow 8$ as a function of the applied magnetic field H_0 . The energy calculated within the London limit (with $a = 1$) starts to depart from the GL results as soon as $L = 1$. This is mainly due to the fact that the usual London theory neglects the spatial variation of $|\Psi^2|$. When the magnetic field increases,

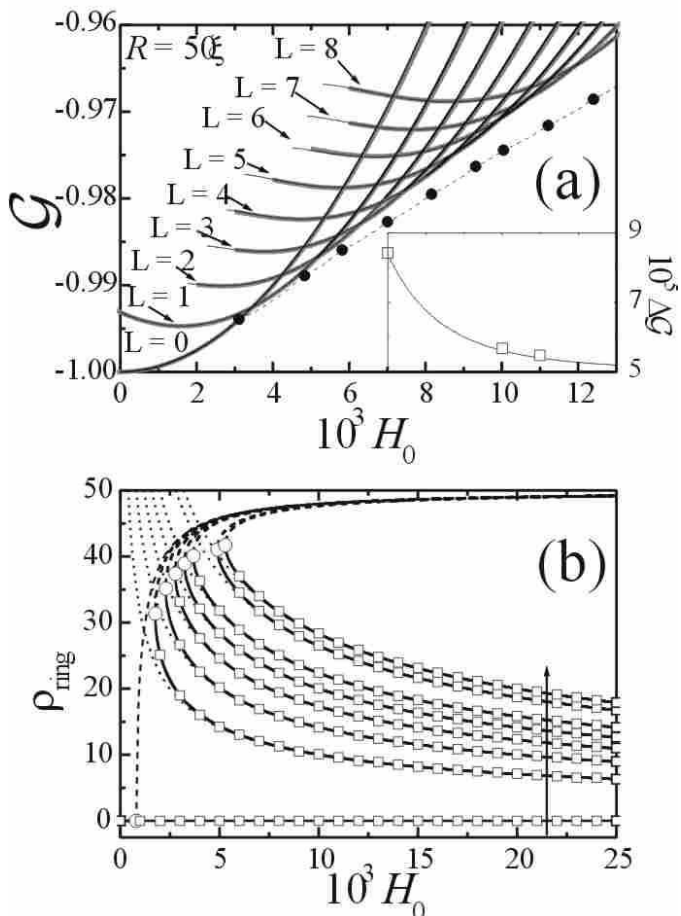


FIG. 2: (a): The GL (thick lines) and the improved London (thin lines) free energies as function of the applied field H_0 for low L -states. The $L = (1, 5)$ state has slightly lower energy than the $L = (6)$ state, as seen in the inset, where the lines and the squares show the difference between the $L = (6)$ and $L = (1, 5)$ energies in the London limit and in the GL theory, respectively. The usual London energy (where we added -1) is also depicted (dashed lines) for comparison. The solid circles show the points at which the usual London energy predicts a transition from L to $L+1$. (b): the GL (open squares) and London (solid lines) radial position of the vortices in the ring (ρ_{ring}) as function of the magnetic field for the $L = 1, (2), (3), (4), (5), (6), (1, 6), (1, 7)$ states. The arrow indicates the direction of increasing L . For each configuration (in the London limit) the vortex position at which the vortex ring is unstable (dashed lines) and the onset field from which stability occurs (open circles) are depicted. The radial positions of the vortex ring when the boundary induced ‘vortex images’ are neglected are shown by the dotted lines for comparison.

the ground state changes by the addition of one vortex, i.e. $L = 0 \rightarrow 1 \rightarrow 2 \dots \rightarrow 8$ (for the London limit these transitions are marked by the filled circles). For disks with small radius the GL theory predicts that $L = 2 \rightarrow 6$ states do not have a vortex in the center of the disk.^{20,24} Such a central vortex appears in the $L = 7 \rightarrow 9$ -states. In contrast, for the present large disk case ($R = 50\xi$), the GL theory and the London approximation yield five

vortices arranged in a regular pentagon with one in the center of the disk for $L = 6$. The state with six vortices in a regular hexagon has a slightly higher energy [the difference in energy is depicted in the inset of Fig. 2(a)].

In an effort to remedy the differences in the energy between the GL and the usual London results we considered the contribution of the vortex cores energies to the London energy. As long as vortices are well separated and $H_0 \ll 1$ ($|\Psi|^2 \approx 1$ far from the vortex cores), Eq. (4c) can be approximately given by the London energy. In this limit the depreciation of $|\Psi|^2$ around the vortex cores can be approximated by the superposition of some function which varies from 0 to 1 within $|\rho - \rho_i| \sim \xi$. Such extensions of the London theory were previously considered^{49,50} for infinite superconducting systems, e.g., by using $|\Psi|^2 = |\rho - \rho_i|^2 / (|\rho - \rho_i|^2 + 2\xi^2)$ close to the core of the vortex at ρ_i . We used this expression into Eq. (4b) in the limit that vortices are far apart, i.e., for low L values, where we can make use of the superposition principle. First, Eq. (4b) can be written as

$$\mathcal{G}_{\text{core}} = -1 + \frac{1}{\pi R^2} \int \left[(1 - |\Psi|^2)^2 + 2(\nabla|\Psi|)^2 \right] d^2\rho. \quad (19)$$

Close to the cores, $1 - |\Psi|^2 = 2 / (|\rho - \rho_i|^2 + 2)$ and $\nabla|\Psi| = 2 / (|\rho - \rho_i|^2 + 2)^{3/2}$ (remembering that $\xi = 1$ in our units). Since these expressions rapidly approach zero, we approximated the integration over the disk area in Eq (19) by the sum of integrations around of the vortex cores. This yields

$$\mathcal{G}_{\text{core}} \approx -1 + L \frac{3}{R^2}. \quad (20)$$

We added the above value of $\mathcal{G}_{\text{core}}$ to the London energy, \mathcal{G}_L , assuming that the vortex core have a radius $\sqrt{2}\xi$, which yields $a = \sqrt{2}$ in ϵ^{core} . The resulting improved London energies are presented in Fig. 2(a) by thin lines for the $L = 1, (2), (3), (4), (5), (1, 5), (1, 6),$ and $(1, 7)$ states. The agreement between this improved London theory with the GL results is very good. Such extension of the London limit yields the region over which each configuration is the ground state with much more confidence than the usual London limit.

In the above approximation for $\mathcal{G}_{\text{core}}$ the depreciation of the order parameter near the disk edge was neglected. In order to have an estimate of the behavior of $|\Psi|^2$ close to $\rho = R$, we may consider the first GL equation written as

$$-\nabla^2\Psi + \Psi(1 - |\Psi|^2 - \Pi^2) = 0, \quad (21)$$

with boundary conditions $\frac{\partial|\Psi|}{\partial\rho}|_{\rho=R} = 0$ and $\hat{\rho} \cdot \Pi|_{\rho=R} = 0$. Notice that $\Pi = \nabla\theta - \mathbf{A} = \boldsymbol{\nu} - \mathbf{A}$ automatically satisfies its boundary condition if $\boldsymbol{\nu}$ is considered within the London limit [cf. Eq. (8)]. For a giant vortex state, $|\Psi|^2$ is radially symmetric, and $\boldsymbol{\nu} = \hat{\phi}L/\rho$. For a regular

polygon vortex configuration and after averaging ν along the angular direction, one finds $\nu = \dot{\phi}L\Theta(\rho - \rho_{\text{ring}})/\rho$, where $\Theta(x)$ is the Heaviside step function. Therefore, one may approximate the superconducting electron density by $|\Psi_{\text{app}}|^2 \approx 1 - (L/\rho - \rho H_0/2)^2$ inside a ring with internal radius, R_1 , taken somewhat larger than ρ_{ring} and external radius smaller than $R - \xi$ (since the term $\nabla^2\Psi$ in the first GL equation becomes more important within distances of ξ close to the disk edge). $|\Psi_{\text{app}}|^2$ is minimal at $\rho = R$ and consequently we can use its value at the boundary in order to estimate when the depreciation of $|\Psi|^2$ close to the edge becomes important (notice that the actual $|\Psi|^2$ is higher close to the disk edge than our approximate result, since there is a correction of order $\nabla^2\Psi/\Psi$, with $\nabla^2\Psi > 0$, in this region). We found that a 5% depreciation in $|\Psi_{\text{app}}(R)|^2$ (which would mean $|\Psi(R)|^2 > 0.95$), requires that $H_0 \approx 0.009$ for $L = 0$, $H_0 \approx 0.0098$ for $L = 1$, $H_0 \approx 0.0106$ for $L = 2$, $H_0 \approx 0.0114$ for $L = 3$, $H_0 \approx 0.0122$ for $L = 4$, $H_0 \approx 0.013$ for $L = 5$, $H_0 \approx 0.0138$ for $L = 6$, $H_0 = 0.0146$ for $L = 7$ and $H_0 = 0.0154$ for $L = 8$, which are magnetic field values well above the respective regions where each of these states are the ground state. Also the order parameter depreciation close to the disk edge results in a less rapid increment of the energy of each L -state compared with the energy found within the London limit. But for $H_0 \ll H_{c2}$, such difference only becomes pronounced at fields well above the magnetic field region over which the respective L -state is the ground state. Nevertheless, the depreciation of the order parameter close to the edges is important if one wishes to understand the entry and exit of vortices in a finite system.

IV. HIGH L -STATES: ABRIKOSOV LATTICE

For large values of the vorticity an Abrikosov lattice appears in the interior of the disk. In this section we will consider $H_0 > 0.03$ and investigate from which value of L the Abrikosov lattice start to occupy a substantial area in the center of the disk.

One difficulty which arises when studying the high L -states is due to the fact that the energy difference between two different L -states and the energy difference between distinct configurations with the same L can be comparable and very small. This is illustrated in Fig. 3, where the energy of the meta-stable states obtained in the London limit at $H_0 = 0.1$ and at $H_0 = 0.2$ are shown. For instance, the difference between the two lowest energy $L = 110$ and $L = 112$ states is less than 10^{-4} . At $H_0 = 0.1$ ($H_0 = 0.2$) we found that a vortex configuration with $L = 111$ ($L = 234$) has the lowest London energy. Of course it is always possible that configurations with lower London energies have not been reached by our simulations (due to the fact that we have a finite number of trials, i.e., we made typically 1000 trials). Nevertheless, the small difference in the energies give us confidence that

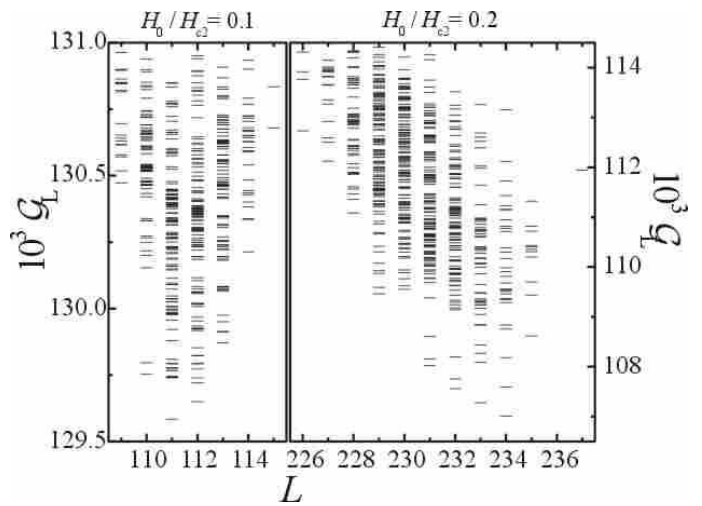


FIG. 3: Energies of the meta-stable states ($L = 109 \rightarrow 115$ and $L = 226 \rightarrow 237$) obtained from simulations within the London limit at $H_0/H_{c2} = 0.1$ (left) and $H_0/H_{c2} = 0.2$ (right). The energy difference between two different L -states is comparable to the energy difference between distinct configurations at the same L -state.

some of these configurations are at least very close to the true ground state within the London limit. Moreover, at such high L values, it is expected that the energy yielded by the London approximation differs considerably from the more realistic results obtained from the GL theory.

In order to circumvent the limitations of the London limit in the calculation of the energy, meta-state states are also investigated within the GL theory. In this case, the correct contribution to the energy from the spatial dependence of $|\Psi(\mathbf{r})|^2$ is taken into account. Again, the question concerning whether the calculated configurations are the true ground states can be addressed, since it is possible that the numerical solution of Eqs. (1,2) becomes trapped in some local minimum. Nonetheless, thermal fluctuations are always present in experiments, making some excited states close to the ground state available for the system. In addition, there is the already mentioned fact that the difference between energies in these high L -states is very small. Therefore, the achievement of the ground state is not crucial for the present study.

Although the London limit fails to give the precise value of the vortex system energy at high L , we expect that the vortex positions obtained within such approach are in good accordance with the GL results (cf. Section II and Ref. 20), at least at fields up to $H_0 \sim 0.2$.^{50,51} Therefore the stability of the ‘London’ configurations within the framework of the GL theory was investigated by solving Eqs. (1) and (2) starting from the given London configuration (usually the ones with lowest energy). By using this procedure, we found that the $L \sim 110$ and $L \sim 230$ configurations, as obtained within the London theory, are also stable within the GL formalism. The calculated GL energies of such configurations are very close

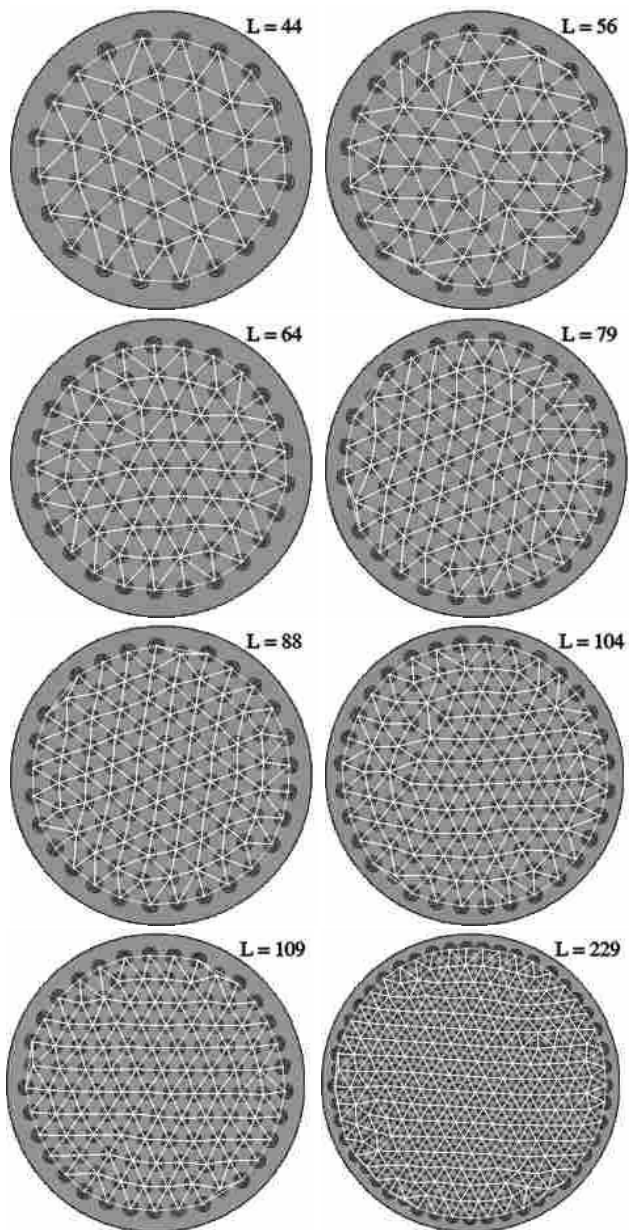


FIG. 4: Superconducting electron density for $L = 44, 56, 64, 79, 88, 104, 109,$ and 229 obtained at $H_0 = 0.04, 0.05, 0.06, 0.07, 0.08, 0.09, 0.10$ and 0.20 , respectively. The white lines depict the Delaunay triangulation for the vortex core positions.

to other GL configurations with the same vorticity, the relative difference lying typically between $10^{-4} - 10^{-5}$. Such values are usually 5 to 10 times smaller than the relative energy difference between the L and $L+1$ lowest energy states.

Some of the stable configurations at $H_0 = 0.04, 0.05, 0.06, 0.07, 0.08, 0.09, 0.10$ and 0.20 are depicted in Fig. 4, for $L = 44, 56, 64, 79, 88, 104, 109,$ and 229 , respectively. From the Delaunay triangulation performed for the core positions, it can be seen that a triangular vortex config-

uration in the center of the disk starts to appear as L increases. First, for $L = 64$ and $L = 79$, an hexagonal vortex arrangement starts appearing in the center of the disk. Such arrangement begins occupying a larger area with increasing vorticity. For $L \gtrsim 100$ the Abrikosov lattice is already present in a considerable region inside the disk.

For the high L -states there is a competition between the ring-like structure imposed by the disk geometry, and the hexagonal lattice favored by the vortex-vortex interaction. As a result, rings are generally formed close to the disk edge while an Abrikosov lattice is present in the center of the disk. In order to study the configurations obtained within the GL theory, we computed the positions of the vortex cores from the calculated $|\Psi(\mathbf{r})|^2$.

First we investigate the ringlike structure near the disk edge by computing the number of vortices, N , and the average density of vortices, $\langle \sigma(\rho) \rangle = N(\rho)/2\pi\rho\Delta\rho$, as a function of ρ . These quantities can suggest where ringlike structures are formed, since $N(\rho)$ (as well as $\langle \sigma(\rho) \rangle$) should present sharp peaks where ringlike patterns exist. For this purpose we divided the disk radius into radial strips of length $\Delta\rho = 1.25\xi$ and counted the number of vortices in each of these pieces. $N(\rho)$ and $\langle \sigma(\rho) \rangle$ are shown in Fig. 5 for $L = 109, L = 229, L = 473$ and $L = 717$ at $H_0 = 0.1, H_0 = 0.2, H_0 = 0.4$ and $H_0 = 0.6$, respectively. The $L = 109$ and $L = 229$ were obtained by solving the GL equations starting with the $L = 110$ and $L = 230$ less energetic configurations calculated within the London limit. We also plotted the respective configurations inside each figure. To help the visualization, rings were drawn for the two outermost shells and a Delaunay triangulation was made for the vortices in the interior of these rings. Clearly, both $N(\rho)$ and $\langle \sigma(\rho) \rangle$ have one sharp peak near the disk edge, an indication of a ring-like structure. This can be observed in the vortex configurations since the outermost vortices are almost perfectly aligned in a ring. For the $L = 109$ state, both $N(\rho)$ and $\langle \sigma(\rho) \rangle$ have additional peaks in the interior of the disk. As the vortex configuration also indicates, this could be interpreted as a second (deformed) outer ring with a somewhat deformed hexagonal lattice in the center. For $L = 229$, it is clear that vortices are distributed in ring-like structures for the two outermost rings with an inner Abrikosov lattice. Similar features are present in the other $L \sim 110$ and $L \sim 230$ vortex states, i.e., sharp peaks near the disk edge are also present in $N(\rho)$ and $\langle \sigma(\rho) \rangle$, indicating two outermost ringlike vortex distribution with an Abrikosov lattice in the center (again this Abrikosov lattice is much better defined for $L \sim 230$). It is also worth to mention that the two outer peaks present at $L \sim 110$ and $L \sim 230$ are situated around the same values of ρ for configurations calculated within both the GL and the London theories. For example, for $L = 109$ the peaks are at $\rho \approx 35$ and $\rho \approx 43$, with an empty region around $\rho \approx 39$ and another for $\rho > 45$. Moreover the regions comprised by the peaks in $\langle \sigma(\rho) \rangle$ at $\rho \approx 35$ and $\rho \approx 43$ contain 28 and 33 vortices, respectively. In the

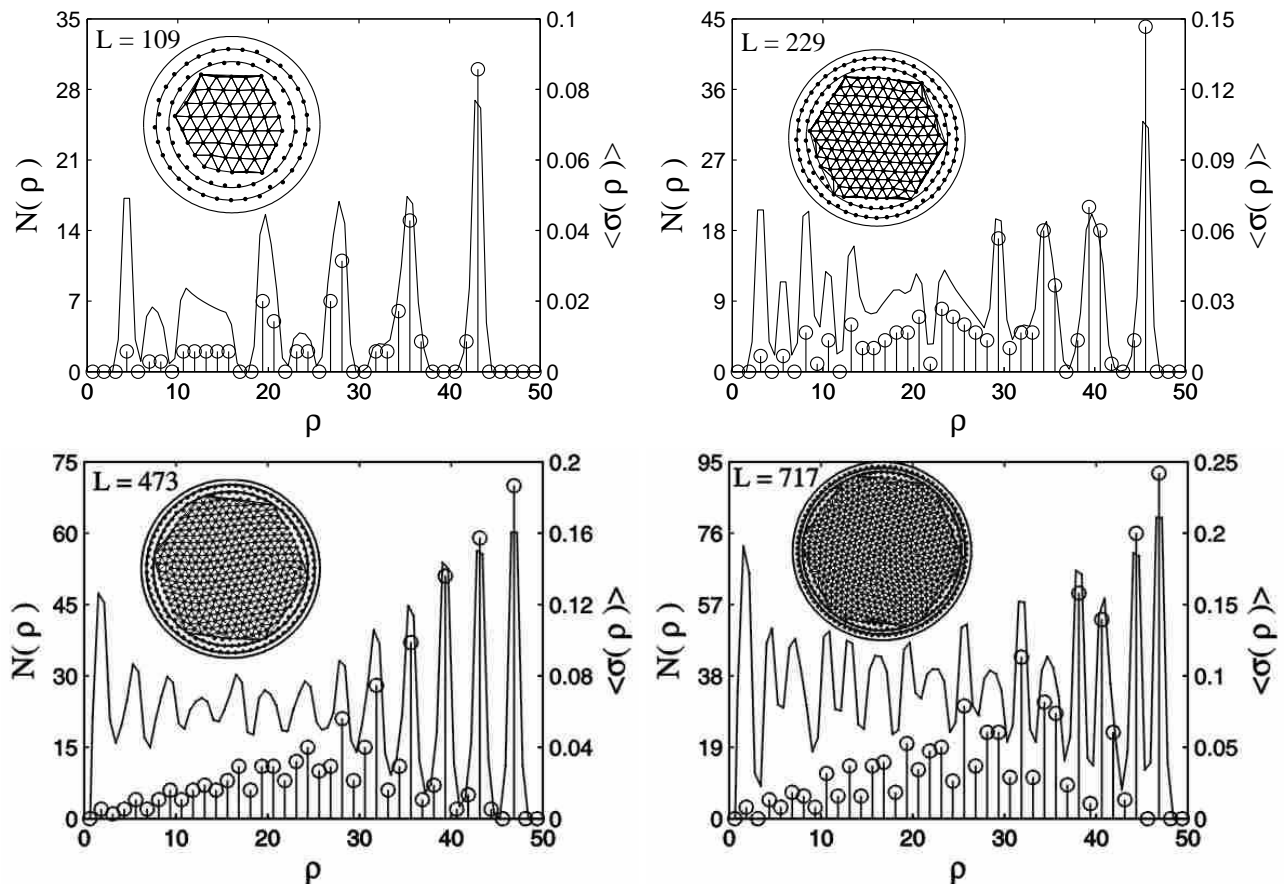


FIG. 5: Number of vortices $N(\rho)$ (circles) and the average vortex density $\langle \sigma(\rho) \rangle$ (solid line) for $L = 109$, $L = 229$, $L = 473$ and $L = 717$ at, respectively, $H_0 = 0.1$, $H_0 = 0.2$, $H_0 = 0.4$ and $H_0 = 0.6$. The respective configurations are depicted in the insets. The well-defined peaks close to $R = 50\xi$ is indicative of a ringlike structure close to the edge. This is also indicated by the configurations in the insets, where we plotted rings for the two outermost shells and the Delaunay triangulation for the inner vortices.

case $L = 229$ one sharp peak occurs around $\rho \approx 46$. The radial region close to this peak contains 48 vortices, with no vortices for $\rho > 47$. The radial region around the peak at $\rho \approx 40$ has 44 vortices, with the region between these two maxima, around $\rho \approx 43$, also vortex free. A more complete description of the number of vortices in the two outer rings is presented in Table I. Taking the number of vortices in the first and second outermost rings for the configurations given in this Table, as well as other configurations not shown here with the same vorticity, we find that the number of vortices in these shells are around, respectively, $33 - 34$ and 28 ± 1 for $L \sim 110$ (50 ± 2 and 45 ± 1 for $L \sim 230$).

In Fig. 5 the states $L = 473$, at $H_0 = 0.4$ and $L = 717$, at $H_0 = 0.6$, are also depicted. As expected, the peaks become broader deep inside the disk, suggesting that the ring-like structure smears out as one approaches the center of the disk. In addition, as the value of L increases the average density becomes more uniform, but preserving at least two sharp peaks near the edge. For $L = 473$ and $L = 717$ the most external ring is situated at $\rho \approx 47$

TABLE I: Number of vortices (N) and approximate radial position of the two outer shells ($\langle \rho \rangle$), and the bond-angular order factor G_6 for configurations with lower energy. Here (i) means all vortices, except the ones belonging to the outermost shell; (ii), vortices not at the two outer rings and (iii) vortices at $\rho \leq 25$.

L	H_0	1st. shell		2nd. shell		G_6		
		N	$\langle \rho \rangle$	N	$\langle \rho \rangle$	(i)	(ii)	(iii)
109	0.1	33	43	28	35	0.76	0.85	0.87
110	0.1	33	43	28	35	0.64	0.71	0.75
111	0.1	33	43	29	36	0.69	0.79	0.84
112	0.1	33	43	29	36	0.68	0.80	0.88
113	0.1	34	43	28	36	0.70	0.80	0.84
229	0.2	48	46	44	40	0.80	0.89	0.97
230	0.2	48	46	44	40	0.78	0.84	0.94
231	0.2	50	46	44	40	0.83	0.92	0.99
232	0.2	49	46	44	40	0.82	0.91	0.97
233	0.2	49	46	45	41	0.80	0.87	0.96
234	0.2	50	46	45	41	0.81	0.87	0.95
235	0.2	49	46	44	41	0.82	0.90	0.97
473	0.4	70	47	66	43	0.79	0.83	0.92
717	0.6	92	47	80	44	0.77	0.79	0.86

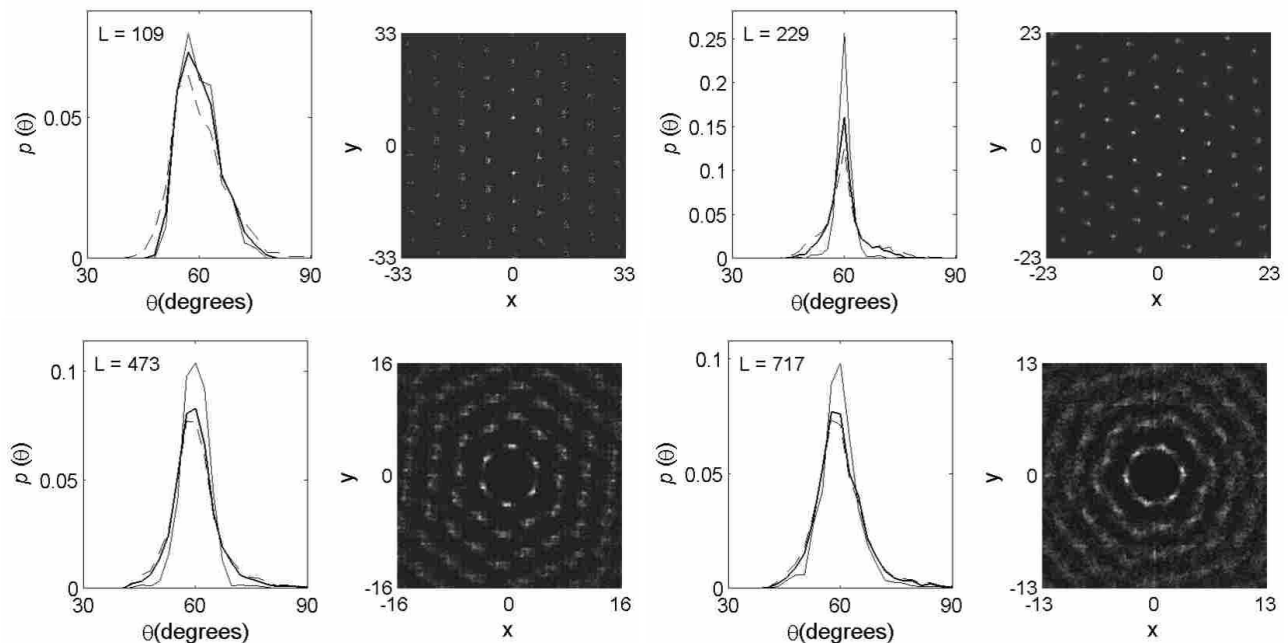


FIG. 6: The density-density correlation function (right) and the probability $p(\theta)$ to find two adjacent nearest neighbors of a given vortex within an angle θ (left) for $L = 109$ at $H_0 = 0.1$, $L = 229$ at $H_0 = 0.2$, $L = 473$ at $H_0 = 0.4$, and $L = 717$ at $H_0 = 0.6$. The dashed, solid, and thin solid lines represent $p(\theta)$ calculated for vortices (i) not in the outermost ring, (ii) not in the two outer rings, and (iii) at $\rho \leq 25$, respectively.

and contains 70 and 92 vortices, respectively. Notice that the two outer rings have a very different number of vortices which is quite distinct from the situation of classical charges confined by a parabolic potential⁴³ where for large number of charges the outer rings contain the same number of particles. The present situation is between a hard wall⁵² and a parabolic confinement case.

We calculated the density-density correlation function for the vortices sitting inside the two outermost rings in order to help characterize whether a Abrikosov lattice is formed away from the disk edge. This quantity is depicted at the right side of Fig. 6. The density-density correlation function indicates an hexagonal pattern for all these high L -states. Such pattern is well defined for $L = 109$ at $H_0 = 0.1$ and becomes very well defined for $L = 229$ at $H_0 = 0.2$. Other configurations with $L \sim 110$ have also an hexagonal pattern as the one for $L = 109$ (but not as sharp). The density-density correlation function computed for various configurations with $L \sim 230$ also resembles the one depicted here for $L = 229$. For $L = 473$ and $L = 717$ the hexagonal pattern is also observed, but not as sharp as the one for $L = 229$. Particularly for the $L = 717$ configuration, the density-density correlation function suggests that each vortex (inside the two outermost rings) still have coordination number equals to six, although the hexagonal structure considering the farther neighbors is not well defined. Therefore these two configurations may still have local, but not orientational order beyond some few neighbors. We shall come back to this point later in Section V,

when discussing the defects in the vortex lattice.

From the density-density correlation function it is also worth to compute the typical inter-vortex distance, a_v , for the vortices forming the Abrikosov lattice. We thus obtained $a_v \approx 8$ for $L = 109$ at $H_0 = 0.1$, $a_v \approx 5.8$ for $L = 229$ at $H_0 = 0.2$, $a_v \approx 4.1$ for $L = 473$ at $H_0 = 0.4$, and $a_v \approx 3.4$ for $L = 717$ at $H_0 = 0.6$.

In order to better describe how close the system is to an Abrikosov lattice we computed the probability distribution, $p(\theta)$, to find two adjacent nearest neighbors of a given vortex making an angle θ . This probability was calculated for three different cases: (i) for all vortices, except the ones at the outermost ring; (ii) for the vortices not in the two outer rings, and (iii) for those vortices at $\rho \leq 25$. These probabilities are shown on the left of Figs. 6. We found that $p(\theta)$ (for all the cases (i) \rightarrow (iii)) is maximum close to 60° , which is characteristic of an hexagonal lattice. The width of the distribution rapidly decreases as L increases from ~ 110 to ~ 230 , but increases as L is further incremented. To be more precise, $p(\theta)$ for the $L \sim 110$ (not only the $L = 109$ state which is shown) state obtained within the London limit has a maximum at 57° , but with $\langle \theta \rangle = 60^\circ$ for the cases (i) \rightarrow (iii) ($\langle \rangle$ means average over the vortices included in each case, (i), (ii) or (iii)). The probability distributions for cases (i) \rightarrow (iii) are not sharp, presenting width of about 12° at half of the distribution maximum. Other states with $L \sim 110$ and comparable energy also show similar behavior. Such features can be understood as the result of the contribution to the $p(\theta)$ distribution

from vortices in the border of the Abrikosov lattice region. Since not so many vortices are present in this region for $L \sim 110$, vortices in its border will contribute more strongly to the $p(\theta)$ distribution than for higher L states. Such vortices have to adjust themselves to the ring-like structure more than the inner vortices and, so, it is likely that a few of them may have nearest neighbors within angles less than 60° or, even, coordination number different to six. For $L > 200$, $p(\theta)$ is sharply peaked at $\theta = 60^\circ$, in conformity with the density-density correlation function, signaling an Abrikosov lattice in the interior of the disk.

For completeness we also calculate the bond-angular order factor^{53,54},

$$G_6 = \left\langle \frac{1}{N_{nb}} \sum_{n=1}^{N_{nb}} \exp(iN_{nb}\theta_n) \right\rangle, \quad (22)$$

where $N_{nb} = 6$ is the number of nearest neighbors of a given vortex, θ_n is the angle between two segments joining the given vortex with two adjacent nearest neighbors and $\langle \rangle$ is again the average over the vortices in cases (i), (ii) or (iii). It is clear from Eq. (22) that $G_6 = 1$ for an ideal Abrikosov lattice. In table I G_6 is depicted for some of the configurations we obtained (typically the configurations with lowest energy). The values found for G_6 are larger than 0.9 at the region (iii) for $L \sim 230$, which indicates a configuration very close to an hexagonal lattice. The $L \sim 110$ states obtained at $H_0 = 0.1$ have lower G_6 , which corroborates our previous analysis suggesting that an Abrikosov lattice is formed but not yet occupying a large area inside the disk. Again, for $L = 473$ and $L = 717$ G_6 is not as large as the one calculated at $L \sim 230$, but is still close or larger than 0.9 in region (iii), which indicates that a local orientational hexagonal order is present. In fact for such large L -values G_6 no longer increases and the peak in $p(\theta)$ is slightly broadened due to the appearance of grain boundaries in the Abrikosov lattice as will be shown in the next section.

V. HIGH L -STATES: DEFECTS IN THE VORTEX LATTICE

As a result of the competition between the geometry induced ring-like structure near the disk border and the hexagonal structure in the center, topological defects in the lattice appear in between these two regions (a feature also observed in confined classical systems^{45,55}). In order to study the distribution of these defects in the disk, we applied the Voronoi construction. In an infinite system both the GL theory and the London approach predict a coordination number equal to six and the Voronoi construction would yield hexagonal unit cells for each vortex. In the disk the situation is different, vortices near the edge have to adjust themselves to the boundary. Therefore, topological defects in the vortex lattice will be present. We shall use the term (wedge) disclination for vortices which have a closed unit cell in

the Voronoi construction with coordination number different from six. This difference is called the topological charge of the disclination. Notice that some vortices at the outermost shell have open unit cells in the Voronoi construction. For such vortices the expected number of nearest neighbors should be four. So in order to define the topological defects also for these vortices, the topological charge there is defined as the number of first neighbors minus 4. By such convention it can be shown from Euler's theorem⁵⁵ that the net topological charge in a disk equals -6 . In addition, dislocations (a bounded pair of one $+$ and one $-$ disclinations) may also appear, whose net topological charge is null, in order to adjust the vortex system to a configuration with lower energy.

Fig. 7 shows the Voronoi construction for the $L = 109$ ($H_0 = 0.1$), $L = 111$ ($H_0 = 0.1$), $L = 234$ ($H_0 = 0.2$), $L = 229$ ($H_0 = 0.2$), $L = 473$ ($H_0 = 0.4$), and $L = 717$ ($H_0 = 0.6$). In all of them it is quite clear that an Abrikosov vortex lattice is formed inside the disk, as indicated in previous section, but with the formation of topological defects in the configurations. The net topological charge for all configurations obtained (including the ones not shown here) is always -6 , in accordance with the Euler theorem.⁵⁵ However the total absolute charge can be much larger than 6. Negatively charged disclinations (vortices with coordination number < 6) are always present. Vortices with coordination number > 6 (positive topological charge) appear accompanied by negative topological charges, leading to the formation of dislocations. The defects in the vortex configurations are more suitable to sit in the disk edge or in the region delimiting the Abrikosov lattice and the ring-like structure. Nevertheless, as L increases, dislocations proliferate and form grain boundaries in the region where the hexagonal lattice appears. This is also the reason why the $L = 473$ and $L = 717$ states have smaller G_6 values and less sharper peaks in the $p(\theta)$ distribution than the lower L states, for instance $L \sim 230$. Such feature is also observed in simulations performed by Reefman and Brom³⁷ considering 2000 vortices (although they considered vortices in the London limit without interaction with the disk edge) and in classical systems of charged particles interacting with each other via the Coulomb potential and confined to a parabolic potential.⁴⁵

Koulakov and Shklovskii⁵⁵ described the presence of dislocations in configurations of classical charged particles confined by a parabolic potential as due to two main reasons: the inhomogeneity in the density of particles and the presence of disclinations. The latter (which is always present in an hexagonal arrangement confined to a disk) causes a large deformation in the particle configurations. Dislocations thus appear in order to reduce such deformations, eventually decreasing the energy of the system. Such effect, also called screening, was previously described by Nelson and Halperin⁵³ when studying the melting driven by dislocations in two dimensional systems, and is linked to the lack of translational long-range order in two-dimensional solid systems (although

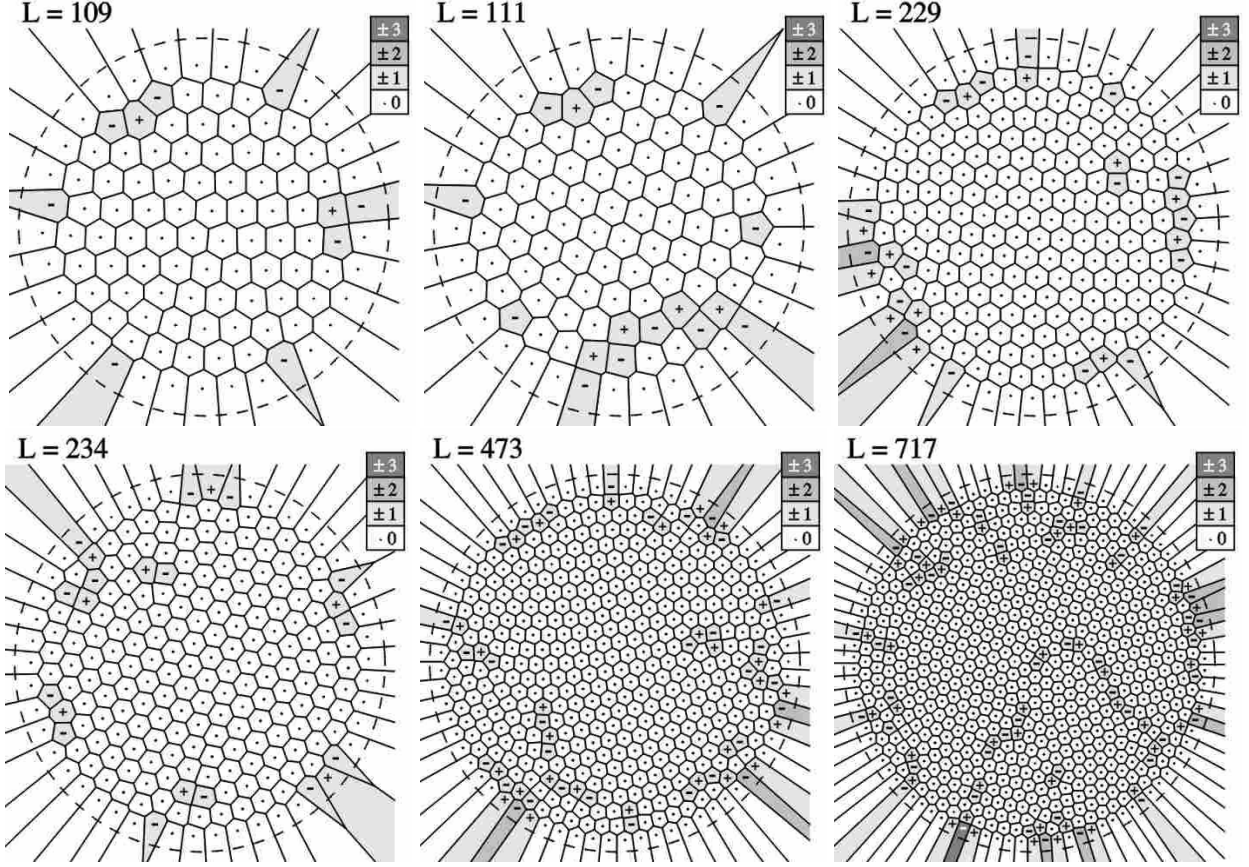


FIG. 7: Voronoi construction for the following configurations: $L = 109$ and $L = 111$ at $H_0 = 0.1$, $L = 229$ and $L = 234$ at $H_0 = 0.2$, $L = 473$ at $H_0 = 0.4$, and $L = 717$ at $H_0 = 0.6$. The dashed line represents the disk edge.

orientational order is still present).⁵⁶ These dislocations are arranged close to or at the disk edge. The former reason induces dislocations in the interior of the disk. In Ref. 55, it was found that there exists a threshold number of particles (which in their case is approximately 700) below which dislocations are due mainly from screening and, above which, such defects appear due to the inhomogeneity of the particle density. At least qualitative similarities exist between such system of charged particles and our vortex configurations. Therefore, it is reasonable to speculate that the same mechanisms which drive the appearance of dislocations is also present here. Just like in the system of charged particles, dislocations are mostly distributed close to and at the disk edge for $L \lesssim 230$ and start proliferating in the Abrikosov lattice for larger L .

Finally, in order to further investigate the relation between defects in the vortex configurations and the energy of the system, we computed the total number of defects (the number of the + and - topological charges) in each stable configuration obtained within the London framework. The results are shown in Figs. 8 for $L = 110$, 111 and 112 at $H_0 = 0.1$ (left) and $L = 230$, 232 and 234 at $H_0 = 0.2$ (right). The absolute value of the net topological charge is depicted as a solid horizontal line

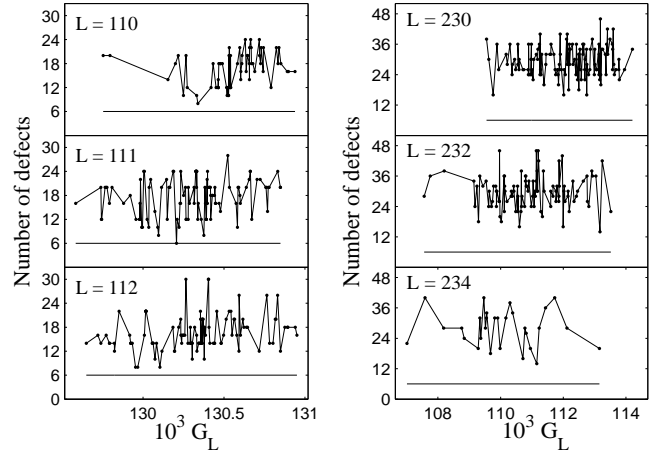


FIG. 8: Number of defects (solid points) versus the energy for some of the configurations obtained from the London approach. The straight horizontal line is the absolute value of the net topological charge.

and is always equal to six as required by the Euler theorem. The total number of defects – which is directly

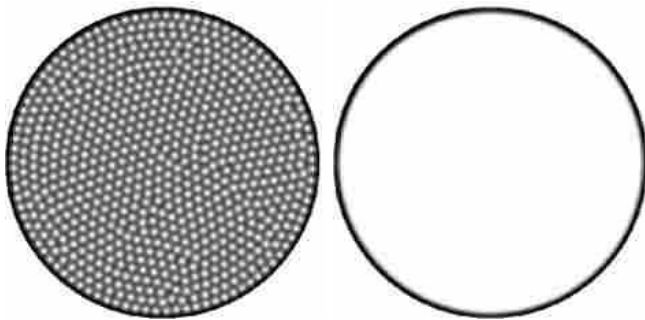


FIG. 9: Superconducting electron density for $H = 0.6$ (left) and $H = 1.02$ (right). White to black runs from low to high values of $|\Psi|^2$.

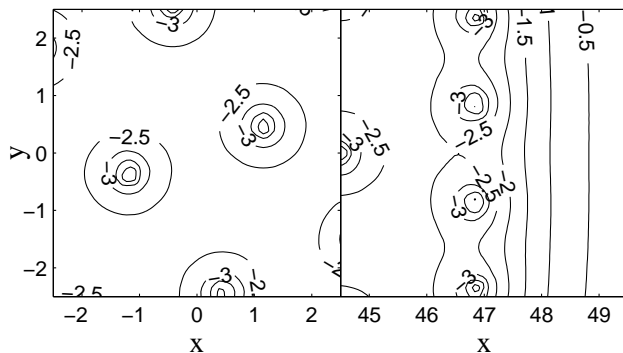


FIG. 10: Contour plots of $\log|\Psi|^2$ at the center (left) and close to the edge of the disk for $H = 1$.

related to the number of dislocations in the configurations – is depicted as points connected by lines. One can notice that the total number of defects is not a monotonic function of the London energy of the configuration. Instead, it highly fluctuates. For example, a configuration free of dislocations (in which only six disclinations occur) almost always has a higher energy than, e.g., one with a total number of 16 topological charges. This happens, for example, for $L = 111$ at $H_0 = 0.1$ where such a configuration with only six disclinations (and no dislocations) has $\mathcal{G}_L = 0.1302066$, which is 0.5% higher than the energy of the lowest energy state, $\mathcal{G}_L = 0.12958384$ (the Voronoi construction of the latter configuration is the $L = 111$ state depicted in Fig. 7). This indicates that the presence, as well as the distribution, of dislocations in the vortex configurations plays an important role in lowering the energy of such configurations.

VI. SURFACE SUPERCONDUCTIVITY

When the external magnetic field approaches $H_0 = 1$ (or $H_0 = H_{c2}$ in not normalized units) the vorticity, L , becomes large. Inside a thin layer close to the disk edge

the superconducting electron density, $|\Psi|^2$, is larger than in the interior of the disk.⁵⁷ Such a behavior may be understood as a result of the superposition of the superconducting electron density depreciation close to each vortex inside the disk, which is less strong for vortices at the surface. This already takes place for $H_0 = 0.6$ with $L = 717$, but is highly pronounced at $H_0 \geq 1.0$. At $H_0 = 0.6$, a multivortex state (as was shown in previous figures and also on the left of Fig. 9) is enclosed by this superconducting sheath. Within this sheath $|\Psi|^2 \approx 0.75$, opposed to a maximum of $|\Psi|^2 \approx 0.5$ between two adjacent vortices. Nevertheless, according to the criterion adopted to characterize the existence of a giant vortex state ($|\Psi|^2 \leq 10^{-4}$ in the region between vortices),²⁰ a giant vortex state appears at $H_0 = 1.02$. In this state $|\Psi|^2 < 10^{-4}$, except at $R - 2\xi < \rho < R$ where $0.2 \leq |\Psi|^2 \leq 0.45$ (cf. Fig. 9 at right). At $H_0 = 1$ the maximum value of $|\Psi|^2$ is $\sim 10^{-2}$ in the region between two adjacent vortex cores, while $|\Psi|^2 \approx 0.55$ at the disk edge. Such a configuration is not yet a giant vortex state, although the multivortex state in this case is extremely ‘dilute’. Possibly $H = 1$ is close to the field in which a giant vortex state decays into a multivortex state.⁵⁸ Moreover, at this magnetic field the depreciation of $|\Psi|^2$ close to the vortex cores is different whether a vortex sits in the outermost ring or in the interior of the disk. This feature is depicted in Fig. 10, where a contour plot of the logarithm of the superconducting electron density is shown in the center of the disk (at left) and close to the edge (at right).

VII. CONCLUSIONS

We investigated the magnetic field dependence of vortex states in thin disks with large radius. The nonlinear GL equations, as well the London approximation were used to obtain stable vortex configurations. Although both methods lead, for small fields, to similar vortex configurations, the energies are different. This is the reason for the failure of the London limit to yield the correct ground state configuration. For low values of the vorticity we improved the London approximation by including the spatial variation of $|\Psi|^2$ close to the vortex cores, which resulted in energies which were very close to those of the GL approach.

Multivortex states were obtained for fields up to $H_0 \approx H_{c2}$, above which a giant vortex state appears. We investigated how the configuration of this multivortex state changes as function of the magnetic field. At low magnetic fields ($H_0 \ll 0.1H_{c2}$) we find vortex configurations having ringlike distribution, as expected from symmetry considerations. However as the number of vortices increases, the vortex-vortex repulsion starts playing a larger role and we observed the appearance of an hexagonal lattice. The ringlike structure is replaced by an Abrikosov lattice in the center of the disk as soon as the field is close to $0.1H_{c2}$, when $L \sim 100$, but is preserved near the edges. For fields larger than 0.1 this Abrikosov

lattice becomes even more pronounced compared to the ringlike structure.

The topological defects in the vortex configurations and their distribution were also studied. We observed two types of defects: (wedge) disclinations and dislocations. The net topological charge is always -6 , as required for an hexagonal structure confined to a circular geometry. Similar to classical particles confined in radially symmetric potentials, we find that these topological defects appear mostly close to the edge for $L \lesssim 230$, in order to adjust the ringlike structure to the Abrikosov lattice. We attribute the presence of dislocations in that region due to the screening of disclinations. As L increases further dislocations start to be spread in the center of the disk and form grain boundaries.

Surface superconductivity was observed at fields around and above $0.6H_{c2}$. This surface superconductivity becomes more pronounced as the vorticity increases, which resulted in a larger overlap between the vortices. We also noticed that the transition from a multivortex to

a giant vortex state takes place at magnetic fields slightly above H_{c2} . Just below the formation of the giant vortex state, the superconducting electron density presents markedly distinct spatial dependence close to the disk edge – where the vortex structure starts to coalesce – compared to what is observed in the center of the disk.

Acknowledgments

This work was supported by the Flemish Science Foundation (FWO-VI), the “Onderzoeksraad van de Universiteit Antwerpen” (GOA), the “Belgian Science Policy”, the European ESF-Vortex Matter, and the Brazilian Science Agency CAPES. One of us (BJB) acknowledges support from FWO-VI and the Japanese Society for the Promotion of Science. We acknowledge useful discussions with C. C. de Souza Silva and M. V. Milošević.

-
- * Electronic address: leonardo.cabral@ua.ac.be
 † Electronic address: ben.baelus@ua.ac.be; Present address: Institute of Materials Science, University of Tsukuba, Tsukuba 305-8573, Japan
 ‡ Electronic address: francois.peeters@ua.ac.be
- ¹ L. D. Landau and E. M. Lifshitz, *Fluid Mechanics, volume 6 of Course of Theoretical Physics* (Pergamon Press, 1987), 2nd ed.
 - ² D. R. Tilley and J. Tilley, *Superfluidity and Superconductivity* (IOP Publishing Ltd., 1990), 3rd ed.
 - ³ M. R. Matthews, B. P. Anderson, P. C. Haljan, D. S. Hall, C. E. Wieman, and E. A. Cornell, Phys. Rev. Lett. **83**, 2498 (1999).
 - ⁴ F. Dalfovo, S. Giorgini, L. P. Pitaevskii, and S. Stringari, Rev. Mod. Phys. **71**, 463 (1999).
 - ⁵ A. L. Fetter and A. A. Svidzinsky, J. Phys. Cond. Mat. **13**, R135 (2001).
 - ⁶ A. A. Abrikosov, Soviet Phys. JETP **5**, 1174 (1957), *ibid.*, Phys. Chem. Solids **2**, 199 (1957).
 - ⁷ A. A. Abrikosov, *Fundamentals of the theory of metals* (North-Holland, 1986).
 - ⁸ E. H. Brandt, J. Vanacken, and V. V. Moshchalkov, Physica C **369**, 1 (2002).
 - ⁹ E. H. Brandt, Phys. Rev. Lett. **78**, 2208 (1997).
 - ¹⁰ E. H. Brandt, Phys. Rev. B **68**, 054506 (2003).
 - ¹¹ V. L. Ginzburg and L. Landau, Zh. Eksp. Teor. Fiz. **32**, 1064 (1950).
 - ¹² A. L. Fetter, P. C. Hohenberg, and P. Pincus, Phys. Rev. **147**, 140 (1966).
 - ¹³ A. L. Fetter and P. C. Hohenberg, Phys. Rev. **159**, 330 (1967).
 - ¹⁴ P. G. de Gennes, *Superconductivity in Metals and Alloys* (Addison-Wesley, Reading, MA, 1989).
 - ¹⁵ J. Pearl, Appl. Phys. Lett. **5**, 65 (1964).
 - ¹⁶ B. J. Baelus and F. M. Peeters, Phys. Rev. B **65**, 104515 (2002).
 - ¹⁷ A. S. Mel'nikov, I. M. Nefedov, D. A. Ryzhov, I. A. Sherevskii, V. M. Vinokur, and P. P. Vyshevlavtsev, Phys. Rev. B **65**, 140503R (2002).
 - ¹⁸ J. J. Palacios, Phys. Rev. B **58**, R5948 (1998).
 - ¹⁹ B. J. Baelus, F. M. Peeters, and V. A. Schweigert, Phys. Rev. B. **63**, 144517 (2001).
 - ²⁰ B. J. Baelus, L. R. E. Cabral, and F. M. Peeters, Phys. Rev. B **69**, 064506 (2004).
 - ²¹ A. K. Geim, I. V. Grigorieva, S. V. Dubonos, J. G. S. Lok, J. C. Maan, A. E. Filippov, and F. M. Peeters, Nature (London) **390**, 256 (1997).
 - ²² P. Singha Deo, V. A. Schweigert, F. M. Peeters, and A. K. Geim, Phys. Rev. Lett. **79**, 4653 (1997).
 - ²³ V. A. Schweigert and F. M. Peeters, Phys. Rev. B **57**, 13817 (1998).
 - ²⁴ V. A. Schweigert, F. M. Peeters, and P. Singha Deo, Phys. Rev. Lett. **81**, 2783 (1998).
 - ²⁵ V. A. Schweigert and F. M. Peeters, Phys. Rev. Lett. **83**, 2409 (1999).
 - ²⁶ P. Singha Deo, V. A. Schweigert, and F. M. Peeters, Phys. Rev. B **59**, 6039 (1999).
 - ²⁷ P. Singha Deo, F. M. Peeters, and V. A. Schweigert, Superlatt. and Microstruct. **25**, 1195 (1999).
 - ²⁸ S. V. Yampolskii and F. M. Peeters, Phys. Rev. B **62**, 9663 (2000).
 - ²⁹ A. K. Geim, S. V. Dubonos, I. V. Grigorieva, K. S. Novoselov, F. M. Peeters, and V. A. Schweigert, Nature (London) **407**, 55 (2000).
 - ³⁰ J. J. Palacios, Phys. Rev. Lett. **84**, 1796 (2000).
 - ³¹ J. Bonča and V. V. Kabanov, Phys. Rev. B **65**, 012509 (2001).
 - ³² T. Mertelj and V. V. Kabanov, Phys. Rev. B **67**, 134527 (2003).
 - ³³ L. F. Chibotaru, A. Ceulemans, V. Bruyndoncx, and V. Moshchalkov, Nature(London) **408**, 833 (2000), *ibid.*, Phys. Rev. Lett. **86**, 1323 (2001); V. R. Misko, V. M. Fomin, J. T. Devreese and V. V. Moshchalkov, Phys. Rev. Lett. **90**, 147003 (2003).

- ³⁴ A. L. Fetter, Phys. Rev. B **22**, 1200 (1980).
- ³⁵ A. I. Buzdin and J. P. Brison, Phys. Lett. A **196**, 267 (1994).
- ³⁶ A. Buzdin and M. Daumens, Physica C **294**, 257 (1998), *ibid.* **332**, 108 (2000).
- ³⁷ D. Reefman and H. B. Brom, Physica C **183**, 212 (1991).
- ³⁸ P. A. Venegas and E. Sardella, Phys. Rev. B **58**, 5789 (1998).
- ³⁹ C. C. d. S. Silva, L. R. E. Cabral, and J. A. Aguiar, Phys. Rev. B **63**, 4526 (2001).
- ⁴⁰ E. Sardella, M. M. Doria, and P. R. S. Netto, Phys. Rev. B **60**, 13158 (2000).
- ⁴¹ R. Kato, Y. Enomoto, and S. Maekawa, Phys. Rev. B **47**, 8016 (1993).
- ⁴² E. H. Brandt, Phys. Rev. Lett. **74**, 3025 (1995).
- ⁴³ V. M. Bedanov and F. M. Peeters, Phys. Rev. B **49**, 2667 (1994).
- ⁴⁴ V. A. Schweigert and F. M. Peeters, Phys. Rev. B **51**, 7700 (1995).
- ⁴⁵ M. Kong, B. Partoens, and F. M. Peeters, Phys. Rev. E **67**, 021608 (2003).
- ⁴⁶ B. Partoens and F. M. Peeters, J. Phys.: Condens. Matter **9**, 5383 (1997).
- ⁴⁷ Y. J. Lai and L. I., Phys. Rev. E **60**, 4743 (1999).
- ⁴⁸ J. Bardeen and M. J. Stephen, Phys. Rev. **140**, 1197A (1965).
- ⁴⁹ J. R. Clem, J. Low Temp. Phys. **18**, 427 (1975).
- ⁵⁰ E. H. Brandt, Rep. Prog. Phys. **58**, 1465 (1995).
- ⁵¹ E. H. Brandt, J. Low. Temp. Physics **26**, 735 (1977).
- ⁵² M. Kong, B. Partoens, A. Matulis, and F. M. Peeters, Phys. Rev. E **69**, 036412 (2004).
- ⁵³ B. I. Halperin and D. R. Nelson, Phys. Rev. Lett. **41**, 121 (1978).
- ⁵⁴ I. V. Schweigert, V. A. Schweigert, and F. M. Peeters, Phys. Rev. Lett. **82**, 5293 (1999).
- ⁵⁵ A. A. Koulakov and Shklovskii, Phys. Rev. B **57**, 2352 (1998).
- ⁵⁶ N. D. Mermin, Phys. Rev. **176**, 250 (1968).
- ⁵⁷ D. Saint-James and P. G. de Gennes, Phys. Lett. **7**, 306 (1963).
- ⁵⁸ V. V. Moshchalkov, V. Bruyndoncx, and L. Van Look, in *Connectivity and Superconductivity*, Eds. J. Berger and J. Rubinstein (Springer-Verlag, Berlin, 2000), Chapt. 4.